The seismic Superattenuators of the Virgo gravitational waves interferometer

Received 9th June 2010

T. Accadia[11] , F. Acernese[5ac] , F. Antonucci[8a] , P. Astone[8a] , G. Ballardin[2] , F. Barone[5ac] , M. Barsuglia[1] , Th. S. Bauer[13a] , M.G. Beker[13a] , A. Belletoile[11] , S. Birindelli[14a] , M. Bitossi[7a] , M. A. Bizouard[10a] , M. Blom[13a] , C. Boccara[10b] , F. Bondu[14b] , L. Bonelli[7ab] , R. Bonnand[12] , V. Boschi[7a] , L. Bosi[6a] , B. Bouhou[1] , S. Braccini[7a] , C. Bradaschia[7a] , A. Brillet[14a] , V. Brisson[10a] , R. Budzynski[16b] , T. Bulik[16cd] , H. J. Bulten[13ab] , D. Buskulic[11] , C. Buy[1] , G. Cagnoli[3a] , E. Calloni[5ab] , E. Campagna[3ab] , B. Canuel[2] , F. Carbognani[2] , F. Cavalier[10a] , R. Cavalieri[2] , G. Cella[7ab] , E. Cesarini[3b] , E. Chassande-Mottin[1] , A. Chincarini[4] , F. Cleva[14a] , E. Coccia[9ab] , C. N. Colacino[7ab] , J. Colas[2] , A. Colla[8ab] , M. Colombini[8b] , A. Corsi[8a] , J.-P. Coulon[14a] , E. Cuoco[2] , S. D'Antonio[9a] , V. Dattilo[2] , M. Davier[10a] , R. Day[2] , R. De Rosa[5ab] , G. Debreczeni[17] , M. del Prete[7ac] , L. Di Fiore[5a] , A. Di Lieto[7ab] , M. Di Paolo Emilio[9ac] , A. Di Virgilio[7a] , A. Dietz[11] , M. Drago[15cd] , V. Fafone[9ab] , I. Ferrante[7ab] , F. Fidecaro[7ab] , I. Fiori[2] , R. Flaminio[12] , J.-D. Fournier[14a] , J. Franc[12] , S. Frasca[8ab] , F. Frasconi[7a] , A. Freise[*] , M. Galimberti[12] , L. Gammaitoni[6ab] , F. Garufi[5ab] , M. E. Gáspár[17] , G. Gemme[4] , E. Genin[2] , A. Gennai[7a] , A. Giazotto[7a] , R. Gouaty[11] , M. Granata[1] , C. Greverie[14a] , G. M. Guidi[3ab] , J.-F. Hayau[14b] , H. Heitmann[14] , P. Hello[10a] , S. Hild[**] , D. Huet[2] , P. Jaranowski[16e] , I. Kowalska[16c] , A. Królak[16af] , N. Leroy[10a] , N. Letendre[11] , T. G. F. Li[13a] , M. Lorenzini[3a] , V. Loriette[10b] , G. Losurdo[3a] , E. Majorana[8a] , I. Maksimovic[10b] , N. Man[14a] , M. Mantovani[7ac] , F. Marchesoni[6a] , F. Marion[11] , J. Marque[2] , F. Martelli[3ab] , A. Masserot[11] , C. Michel[12] , L. Milano[5ab] , Y. Minenkov[9a] , M. Mohan[2] , J. Moreau[10b] , N. Morgado[12] , A. Morgia[9ab] , S. Mosca[5ab] , V. Moscatelli[8a] , B. Mours[11] , I. Neri[6ab] , F. Nocera[2] , G. Pagliaroli[9ac] , L. Palladino[9ac] , C. Palomba[8a] , F. Paoletti[7a,2] , S. Pardi[5ab] , M. Parisi[5b] , A. Pasqualetti[2] , R. Passaquieti[7ab] , D. Passuello[7a] , G. Persichetti[5ab] , M. Pichot[14a] , F. Piergiovanni[3ab] , M. Pietka[16e] , L. Pinard[12] , R. Poggiani[7ab] , M. Prato[4] , G. A. Prodi[15ab] , M. Punturo[6a] , P. Puppo[8a] , D. S. Rabeling[13ab] , I. Rácz[17] , P. Rapagnani[8ab] , V. Re[15ab] , T. Regimbau[14a] , F. Ricci[8ab] , F. Robinet[10a] , A. Rocchi[9a] , L. Rolland[11] , R. Romano[5ac] , D. Rosinska[16g] , P. Ruggi[2] , B. Sassolas[12] , D. Sentenac[2] , L. Sperandio[9ab] , R. Sturani[3ab] , B. Swinkels[2] , A. Toncelli[7ab] , M. Tonelli[7ab] , O. Torre[7ac] , E. Tournefier[11] , F. Travasso[6ab] , G. Vajente[7ab] , J. F. J. van den Brand[13ab] , S. van der Putten[13a] , M. Vasuth[17] , M. Vavoulidis[10a] , G. Vedovato[15c] , D. Verkindt[11] , F. Vetrano[3ab] , A Viceré[3ab] , J.-Y. Vinet[14a] , H. Vocca[6a] , M. Was[10a] , M. Yvert[11]

[1] AstroParticule et Cosmologie (APC), CNRS: UMR7164-IN2P3-Observatoire de Paris-Université Denis Diderot-Paris 7 - CEA : DSM/IRFU, France

[2] European Gravitational Observatory (EGO), I-56021 Cascina (Pi), Italy

[3] INFN, Sezione di Firenze, I-50019 Sesto Fiorentino[a] ; Università degli Studi di Urbino 'Carlo Bo',
I-61029 Urbino[b] , Italy

[4] INFN, Sezione di Genova; I-16146 Genova, Italy

[5] INFN, Sezione di Napoli [a] ; Università di Napoli 'Federico II'[b] Complesso Universitario di Monte S.Angelo, I-80126 Napoli; Università di Salerno, Fisciano, I-84084 Salerno[c] , Italy

[6] INFN, Sezione di Perugia[a] ; Università di Perugia[b] , I-6123 Perugia,Italy

[7] INFN, Sezione di Pisa[a] ; Università di Pisa[b] ; I-56127 Pisa; Università di Siena, I-53100 Siena[c] , Italy

[8] *INFN, Sezione di Roma[a] ; Università 'La Sapienza'[b] , I-00185 Roma, Italy*
[9] *INFN, Sezione di Roma Tor Vergata[a] ; Università di Roma Tor Vergata[b] ; Università dell'Aquila, I-67100 L'Aquila[c] , Italy*
[10] *LAL, Université Paris-Sud, IN2P3/CNRS, F-91898 Orsay[a] ; ESPCI, CNRS, F-75005 Paris[b] , France*
[11] *Laboratoire d'Annecy-le-Vieux de Physique des Particules (LAPP), IN2P3/CNRS, Université de Savoie, F-74941 Annecy-le-Vieux, France*
[12] *Laboratoire des Matériaux Avancés (LMA), IN2P3/CNRS, F-69622 Villeurbanne, Lyon, France*
[13] *Nikhef, National Institute for Subatomic Physics, P.O. Box 41882, 1009 DB Amsterdam[a] ; VU University Amsterdam, De Boelelaan 1081, 1081 HV Amsterdam[b] , The Netherlands*
[14] *Université Nice-Sophia-Antipolis, CNRS, Observatoire de la Côte d'Azur, F-06304 Nice[a] ; Institut de Physique de Rennes, CNRS, Université de Rennes 1, 35042 Rennes[b] , France*
[15] *INFN, Gruppo Collegato di Trento[a] and Università di Trento[b] , I-38050 Povo, Trento, Italy; INFN, Sezione di Padova[c] and Università di Padova[d] , I-35131 Padova, Italy*
[16] *IM-PAN 00-956 Warsaw[a] ; Warsaw University 00-681 Warsaw[b] ; Astronomical Observatory Warsaw University 00-478 Warsaw[c] ; CAMK-PAN 00-716 Warsaw[d] ; Bialystok University 15-424 Bialystok[e] ;*
IPJ 05-400 Swierk-Otwock[f] ; Institute of Astronomy 65-265 Zielona Góra[g] , Poland
[17] *RMKI, H-1121 Budapest, Konkoly Thege Miklós út 29-33, Hungary*
[*] *University of Birmingham, Birmingham, B15 2TT, United Kingdom*
[**] *University of Glasgow, Glasgow, G12 8QQ, United Kingdom*

corresponding author: *Federico Paoletti - European Gravitational Observatory (EGO) I-56021 Cascina (Pi), Italy*
e-mail address: *federico.paoletti@pi.infn.it*

ABSTRACT

The Virgo experiment, located near Pisa, Italy, is a large laser Michelson interferometer aiming at the first direct detection of gravitational waves. The interferometer monitors the relative distance of its mirrors placed at the ends of two 3 km-long perpendicular arms. The goal is to measure spectral differential variations of the arm lengths of 10^{-18} m/Hz$^{1/2}$ in the frequency range from 10 Hz to 10 kHz. Avoiding spurious motions of the optical components is therefore essential to detect gravitational waves. Since the ground motion is 9 orders of magnitude larger than the arm length variations induced by gravitational waves, the seismic noise is the dominant low frequency noise source for terrestrial gravitational wave interferometers. The seismic isolation is obtained suspending the mirrors by an 8-meter tall chain of cascaded mechanical filters, called "Superattenuator" (SA). The Superattenuator is a passive device acting as a low pass filter in all six degrees of freedom, capable of attenuating the ground motion by more than 10 orders of magnitude, starting from a few Hz. To further reduce the seismic disturbances, the filter chain is suspended from an actively stabilized platform that compensates for low frequency and large amplitude oscillations caused by the mechanical resonances of the chain. In this article we describe the Superattenuator together with its control system, and we report about its performance.

1. GRAVITATIONAL WAVES AND DETECTORS

According to Einstein is theory of general relativity, tiny "ripples" of space-time, called gravitational waves (GW) are generated by astrophysical processes which involve large accelerated masses, such as supernova explosions, coalescence of binary star systems, spinning neutron stars and the big bang. As they travel at the

speed of light, GW distort space-time in such a way that the distance between free masses will alternatively decrease and increase during the passage of the wave. The effect of a GW impinging perpendicularly on a hypothetical circle of free masses is to alternatively elongate it in one direction and stretch it in the orthogonal direction at the wave frequency. The amplitude of a GW, usually called "strain amplitude", is represented by the dimensionless parameter h that is proportional to the relative variation of the distance between two free masses. The expected amplitude on Earth of GW produced by typical astrophysical sources is approximately $h \sim 10^{-21}$. To appreciate the challenge of GW detection, it should be considered that this strain amplitude would change the distance of two masses placed 1 km apart by less than the size of a proton (10^{-18} m).

In recent years, the first generation of resonant bar GW detectors has been overtaken by more sensitive and broad-band instruments based on the technique of laser interferometry, called GW interferometers[1]. Several of these detectors are currently in operation: the two LIGO detectors[2] at Hanford, WA and Livingston, LA sites in USA, GEO-600[3] in Hannover (Germany), TAMA-300[4] in Japan, and Virgo[5] in Italy. All these detectors have reached their design sensitivity, and have already collected a considerable amount of data which are being analyzed. Some interferometers are now in the process of being upgraded towards more sensitive design (e.g. *Advanced Virgo*, http://wwwcascina.virgo.infn.it/advirgo, will have a sensitivity increased by one order of magnitude between 10 and 100 Hz).

1.1 Optical Design

Figure 1 shows the optical scheme of a typical GW detector. Every GW interferometer is based on the Michelson interferometer. A laser beam is split in two by a semi-reflective mirror (Beam Splitter, BS). The two beams travel in orthogonal directions along the interferometer "arms" up to two distant mirrors which reflect them back to the BS. The recombined beam out of the BS then impinges on a photo-detector. The passage of a gravitational wave causes a differential variation of the arm lengths: one arm stretches while the other elongates. This results in a phase difference between the beams in the two arms, and thus in a change of the intensity of the recombined beam on the photo-detector. The strain sensed by such detector is $h \sim \Delta L / L$, where ΔL is the change in the arm length difference caused by the passage of the GW, and L is the effective optical path of the light in each arm.

In order to increase the optical path length (and thus the strain sensitivity), while keeping the physical arms length within a few kilometers for practical reasons, one uses multiple reflections between two mirrors. This is implemented by placing two additional mirrors (semi-reflective input mirrors, in Figure 1) in order to form two long resonant optical cavities, one per arm.

One additional semi-reflective mirror, Power Recycling in Figure 1, is placed between the laser and the BS. Its role is to reflect back to the interferometer the light that would instead return to the light source and be lost. This technique allows an increase (by a factor 50 in Virgo) in the total light power trapped inside the Interferometer (ITF), consequently reducing the shot noise associated to statistical fluctuations of the number of photons that reach the photo-detector.

To optimize the measurement of ΔL, GW interferometers work as null instruments. This means that the differential arms length is kept to zero by applying an actuation force on the mirrors.

The differential arms length is actively controlled and kept on the *dark fringe*, a condition in which the two output beams are made to interfere out of phase, and in principle no light exits from the detector. In practice, the signal at the output port carries information about the GW, as well as about the noises affecting the interferometer, including the position fluctuations of the mirrors. For this reason, the relative position of several mirrors has to be controlled along several angular and longitudinal degrees of freedom. This is achieved with the implementation of sophisticated control techniques which use as error signals the information carried by light beam fractions extracted at some locations of the optical path.

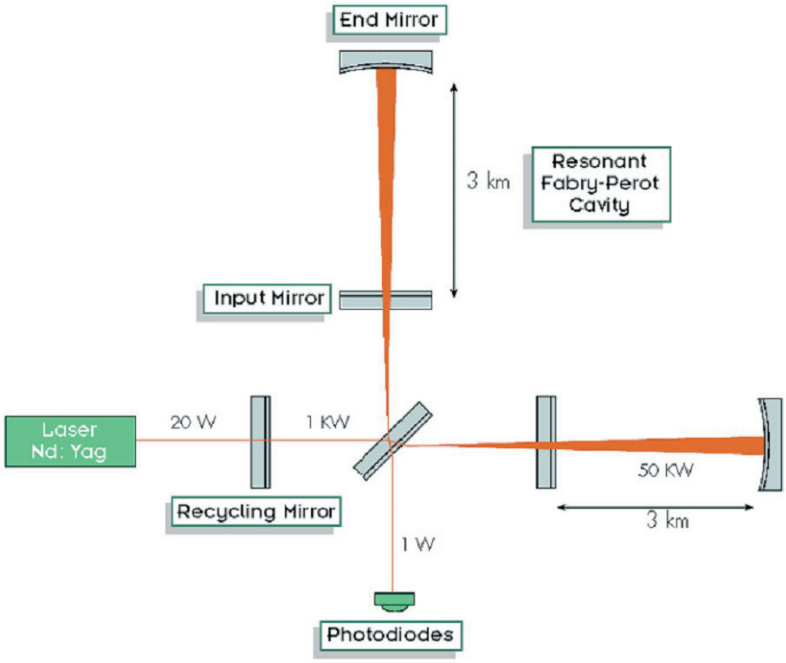

Figure 1. simplified optical scheme of the Virgo interferometer

Figure 2. aerial view of the Virgo interferometer

2. THE VIRGO GW INTERFEROMETER

The Virgo detector, shown in Figure 2, is located in Cascina, near the city of Pisa in Italy, and hosted by the European Gravitational Observatory laboratory. The interferometer is run by an International scientific collaboration founded by the French CNRS and the Italian INFN. Other groups from Holland, Poland, Hungary recently joined the collaboration in order to contribute to the interferometer upgrades. The site has been selected to satisfy the requirement of a low anthropic seismic noise. Moreover the area is kept free from tall vegetation to limit soil vibrations induced by wind.

The Virgo arms are 3 km long, and are approximately oriented along the North and West directions. Virgo design sensitivity curve, the main figure of merit for GW detectors, is shown in Figure 3. It measures the equivalent strain noise produced by several effects that can mimic a gravitational wave signal. With respect to other detectors a peculiarity of Virgo is its remarkably good sensitivity in the frequency region between 10 Hz and 100 Hz ($h = 5\ 10^{-23}/\sqrt{Hz}$ at 100 Hz, and $h = 3\ 10^{-21}/\sqrt{Hz}$

at 10 Hz) where GW signals emitted by slowly rotating neutron stars and by massive coalescing objects are expected. The Virgo detector has actually reached the design sensitivity during the recently completed test run (Figure 4).

2.1 Noise Sources

The major noise sources contributing to the Virgo detector are summarized in Figure 3. We are now going to briefly describe them in the following subsections.

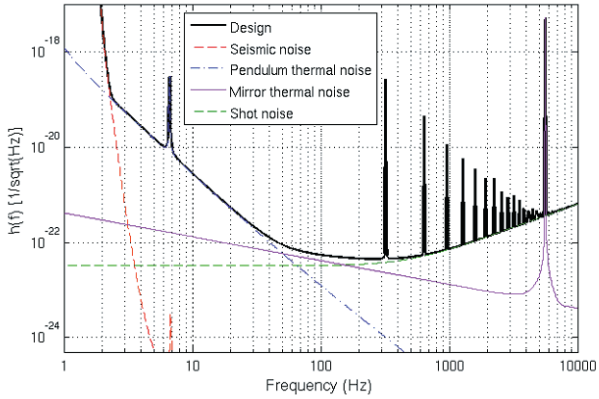

Figure 3. design sensitivity of Virgo, as a function of frequency. Curves in color show the main limiting noises. The shot noise is associated with the statistical fluctuations in the number of photons described in Sec.1.

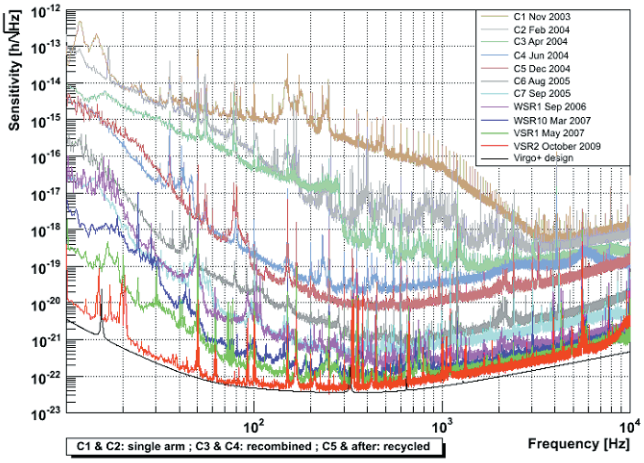

Figure 4. progress in Virgo sensitivity curve from first commissioning (Nov. 2003) to last Scientific Run (Oct. 2009). Solid black curve is the design curve.

2.1.1 Seismic Noise

Since the ground motion is 9 orders of magnitude larger than the arm length variations induced by gravitational waves, the seismic noise is the dominant low frequency noise source for terrestrial gravitational wave interferometers. In VIRGO the required seismic isolation is achieved through a chain of suspended seismic filters, called the Superattenuator, which is described in the following sections.

2.1.2 Thermal Noise

Between 10 Hz and 100 Hz, the sensitivity of Virgo is limited by the mechanical «thermal noise». Each resonance mode of the mirrors and of the suspensions is permanently excited randomly by a thermal force proportional to the square root of

the absolute temperature and inversely proportional to the square root of the quality factor[6]. If these modes are very weakly damped (high Q), their energies are concentrated in very narrow lines around each resonance frequency, and do not spoil the sensitivity at other frequencies. But if a resonance is damped, then the line gets broader, and the thermal force generates a noise which can dominate the whole spectrum. Therefore it has been extremely important, in the design and realization of the SA, to minimize all sources of mechanical damping, by selecting the materials and the right way to connect all the components to avoid friction.

In order to preserve the beam quality, the best available optical elements are employed. The Virgo mirrors combine the highest surface quality (better than a hundredth of a micron) with extremely low diffusion and absorption (less than 1 ppm) Because of the very high optical power accumulated in the various resonant cavities (50 kW are stored in the arms optical cavities), mirrors tend to deform and thus deteriorate the beam quality. Besides the use of low thermal absorption materials, employed for mirrors and coatings, a Thermal Compensation System (TCS) is employed to compensate for these thermal effects. This actively controlled system consists of a pre-stabilized CO_2 laser projector that shines a heating pattern onto the front surface of each arm input mirror.

2.1.3 Pressure fluctuations

If traveling in air, the light beam optical path would be disturbed by the refractive index changes due to statistical fluctuations of gas molecule density, as well as by scattering processes.

For this reason, the whole Virgo apparatus is kept under ultra high vacuum (10^{-10} mbar). Each SA is contained in a vacuum "tower". Towers are linked by vacuum tubes of 1.2 m diameter surrounding the entire beam path. The vacuum also helps suppressing the transmission of acoustic noise to the suspended mirrors. Special care is taken to select vacuum compatible materials. To reduce vacuum contamination all in vacuum components are subject to special baking and cleaning procedures.

2.1.4 Laser Instabilities

The laser beam must be extremely stable in frequency, lateral jitter and power. The Virgo light source belongs to a new generation of ultra-stable lasers. It is a 20 Watt Nd-YVO_4 (wavelength l=1.064μm) laser that is injection-locked to a high-stability Nd:YAG solid state master laser.

Before entering the ITF arms the laser beam circulates inside a suspended resonant optical cavity, called Input Mode Cleaner (IMC). The role of IMC is to suppress all transverse modes different from the fundamental Gaussian one (TEM00), and also to further suppress the jitter and frequency noise.

3. THE VIRGO SUPERATTENUATOR

The Superattenuator (SA) is the seismic isolation system of the Virgo mirrors; its role is to decouple the mirrors from ground so that they can behave as "freely" falling masses.

Constituted by a sequence of several mechanical filters (Figure 6), the SA is able to isolate the interferometer optical components from the seismic noise exploiting the properties of a multistage pendulum. In a multi-stage pendulum, at frequencies above the resonant modes, the horizontal displacement of the suspension point is transmitted to the lowest mass multiplied by a factor C / f^{2N}, where N is the number of stages and C is the product of the square of the N resonant frequencies.

The SA must reduce the ground motion at the mirror level below the mirror thermal noise (see Sec. 2). Given the spectral density of the thermal noise (see Figure 3) and of the typical ground displacement (Figure 5), the SA has to provide a seismic attenuation in the horizontal direction of at least a factor 10^9 starting from a few Hz. In order to obtain this level of isolation, the mechanical resonances of the system have to be kept below 1Hz, that means to build long pendulums.

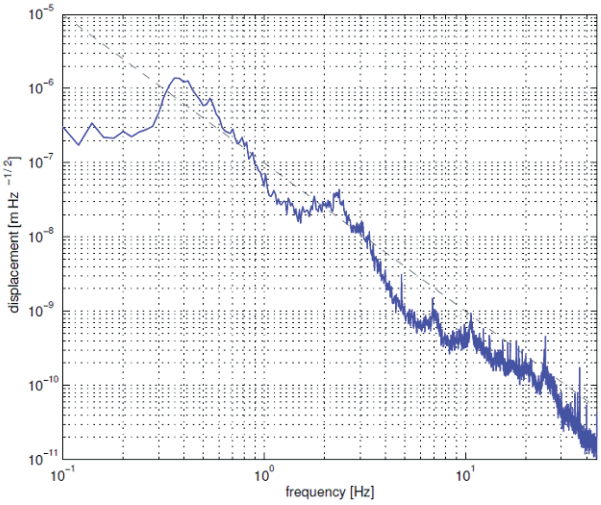

Figure 5. linear spectral density of the horizontal seismic vibration of the ground, measured on the Virgo site; the seismic noise turns out to be roughly isotropic and well approximated by the function 10^{-7} f $^{-2}$m/$\sqrt{\text{Hz}}$ (see dashed line)

The two end mirrors, suspended 3 km away, are misaligned with respect to the plumb line by about 3.10^{-4} rad in order to compensate for the Earth curvature. This implies that a fraction of the chain vertical vibrations is always transmitted along the beam direction. The suspension system causes even larger mechanical couplings (1%), due to structural reasons. The SA must therefore be capable of providing a high attenuation performance along both the horizontal and vertical directions.

The vertical isolation is obtained suspending the masses through vertical elastic elements so as to achieve a chain of oscillators along both horizontal and vertical directions. Thus, the SA vertical isolation is also of the type: C / f^{2N}. A dedicated anti-spring system (described later in sec. 3.3) has been designed to keep the vertical resonances of the system well below a few Hz.

In addition to the pendulum chain, each SA includes a "top stage" and a "payload". The top stage consists of a three leg inverted pendulum with a top platform, and is described in details in sec. 3.1.

The payload consists of an upper mass, called "marionette", supporting the mirror. The marionette supports also a so called "reference mass", suspended behind the mirror and acting as reaction mass for the actuators controlling the mirror position; it is described in details in sec. 3.4.

While for frequencies above a few Hz, the SA is essentially a passive isolation device, between 200 mHz and 2 Hz, i.e. below the Virgo detection band, the seismic excitation is amplified by the normal modes of the filter chain, making the mirror swing along the beam by more than ten microns. Consequently, in order to guarantee the mirror slow swing, the low frequency resonant modes of the chain need to be actively damped. For this reason coil-magnets actuators placed along the SA chain (top stage, marionette, mirror) allow the adjustment of the chain alignment position, and to implement active damping of chain normal modes and hierarchical control (see sec. 4)

Here below we describe in more detail the SA structure and functionality of single chain elements, and their control. Additional information can be found in reference [7].

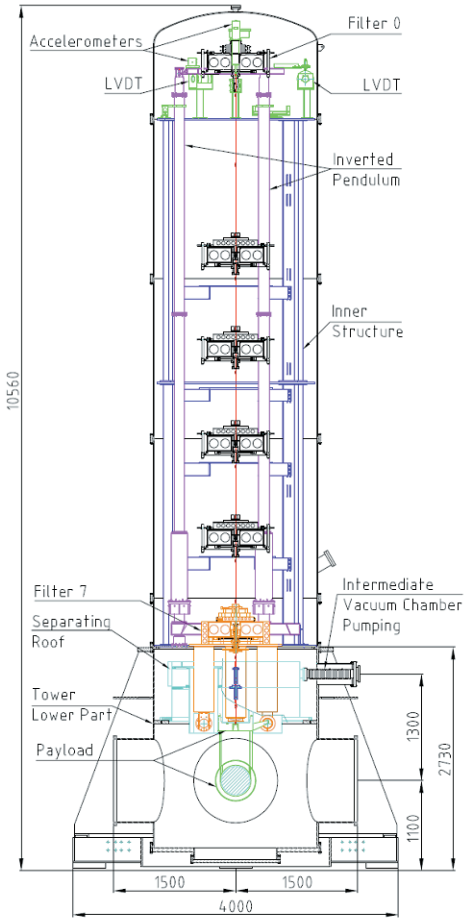

Figure 6. vertical cross-section of a tower, showing inner details and the SA

3.1 The Inverted Pendulum top stage

The top stage of the SA is designed to fulfill three main functions:

- to introduce an additional very low frequency (~40 mHz) horizontal filtering stage;
- to provide the SA with a suspension point positioning system.
- to provide a soft suspension stage on the top of the chain allowing active mode damping and seismic noise reduction by means of inertial sensors, position sensors and electromagnetic actuators. In addition, any noise introduced by acting on the top stage is filtered out by the SA chain.

In order to meet the above requirements, a pre-isolator device based on the working principle of the Inverted Pendulum (IP) has been realized. An IP is a suitable device for two reasons:

- the device can be tuned to a very low frequency (about 40 mHz in Virgo) simply adding a small mass on its top;
- since the force required to displace the chain suspended from an IP resonating at 40 mHz is very low (less than 1 N to move 1 ton SA chain by 1 cm), soft electromagnetic actuators can be used to control the suspension point position.

The IP is therefore a good platform to act upon for the active damping of the SA normal modes.

The Virgo IP (Figure7) consists of three metallic legs connected through flexible joints to a bottom ring resting on ground. A steel ring is suspended to the top end of the three legs by three thin wires (31 mm long). This ring surrounds the first filter of the chain (hereafter called Filter Zero) to which it is rigidly connected.

The Filter Zero together with the top ring form a platform from which the whole pendulum chain is suspended.

Each leg is a 26 kg aluminum pipe with an inner diameter of 125 mm and a 2.5 mm thickness. The total length of the leg, from the bottom of the flexible joint to the suspension point of the SA is about 6.2 m. The leg is composed by two sections flanged together and reinforced with titanium inserts.

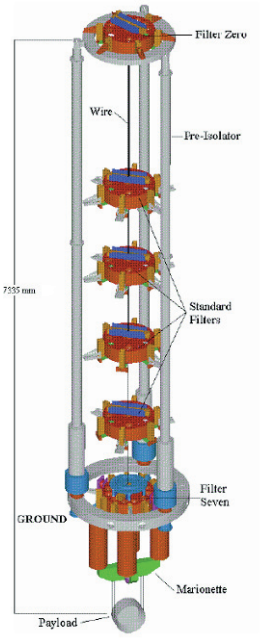

Figure 7. interal view of a tower, showing SA 3D design

The IP structure is surrounded by a rigid metallic structure (called the inner structure, see Figure 8), holding the parts of sensors and actuators that need to be referred at ground.

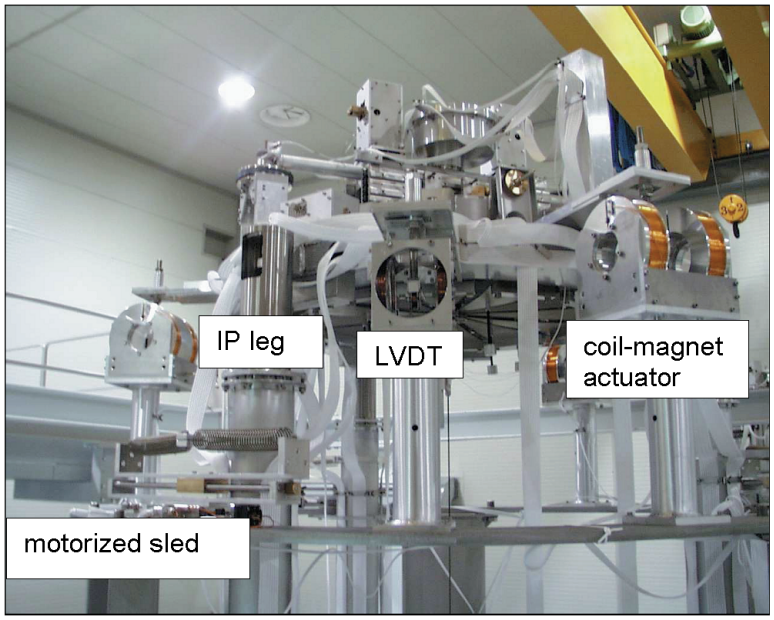

Figure 8. details of IP sensors and actuators.

3.2 The seismic Filters

In the SA each seismic filter consists of a rigid stainless steel cylinder (70 cm diameter, 18.5 cm high for a total weight of about 100 kg) suspended from a point as close as possible to its centre of mass (Figure 9). A set of triangular cantilever spring blades is clamped on the outer circumference of the filter bottom side. Each blade (3.5 mm thick and 385.5 mm long) is bent at a constant curvature radius and with a different base width according to the load to be supported. The different curved blades become flat and horizontal under loads ranging between 48 and 96 kg. Each blade tip is connected by a 1 mm diameter steel piano wire to a mobile central column, coaxial to the filter body. Any movement of the central column, apart from the vertical direction, is prevented by two sets of four centering wires stretched on the top and on the bottom of the filter body.

A crossbar, bolted on the top side of the central column, is used as a mechanical support for the magnetic anti-spring system described in the next section. The central column and the crossbar represent the moving part of the mechanical filter from which the load of the lower stages is suspended by a steel suspension wire. By connecting each filter to the next one, a chain of mechanical oscillators in the vertical direction is obtained.

The set of triangular steel blades mounted under each filter, sustains the weight of the lower part of the chain (Figure 10). The support capability of each spring set is tuned by varying the number of blades from 12 to 4, the base width of each blade between 180 mm and 110 mm and the curvature radius without load.

Once properly loaded, the main vertical resonant frequency of each filter is about 1.5 Hz. In order to reduce the peak amplitude of the blade first flexural mode (at about 110 Hz), a rubber/metal damper is mounted in the middle of each blade.

Another special damper, mounted on the crossbar, suppresses a mode at about 50 Hz, due to the suspension wire connecting the crossbar to the next filter and acting as a stiff spring.

"Maraging" steel has been used in place of standard steel for blade construction in order to minimize micro-creep effects[8] due to the high load applied. We used the same material to machine the suspension wires with nail-heads at both ends. Since the suspended load decreases going from the top to the bottom of the chain, the wire diameter changes along the chain in the range 4 - 1.85 mm.

The two nail-heads of the wires connecting each filter to the upper and to the lower ones are screwed in the central part of the filter body at a relative distance of 5 mm, very close to the filter center of mass. This guarantees a small return torque to rotations of the filter around a horizontal axis and thus a low tilt frequency.

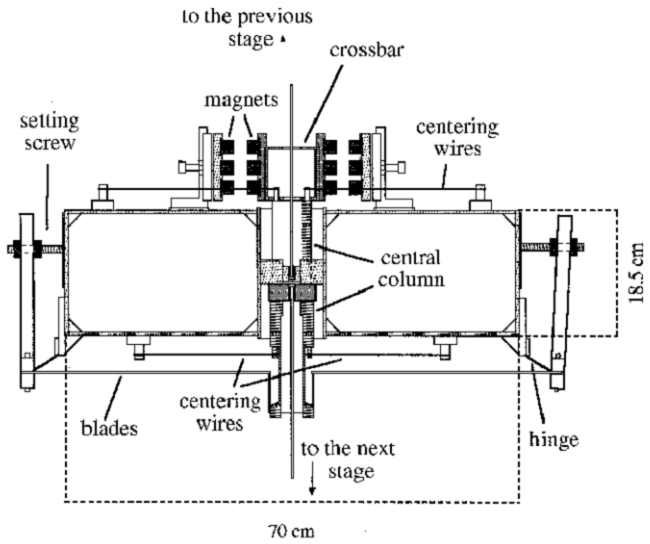

Figure 9. section view of SA vertical mechanical filters

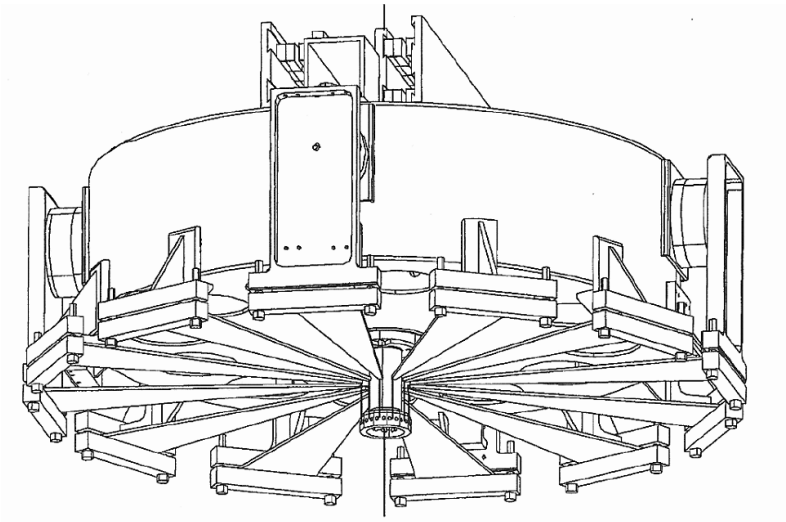

Figure 10. 3D view of SA vertical mechanical filters

3.3 The magnetic anti-spring

The chosen suspension wire length of 1.15 m sets the pendulum resonant frequency of each stage at about 0.5 Hz. In the vertical direction the stiffness of the triangular blade springs fixes the natural resonant frequency at about 1.5 Hz.

In order to reduce the vertical stiffness of the blades, and then to confine the main vertical resonant frequency of each filter below the pendulum one, a system of "magnetic anti-springs"[9, 10] has been conceived. It consists of four sets of permanent magnets (two assembled on the crossbar and two on the filter body) facing each other with opposite horizontal magnetic moment (namely in a repulsive configuration). The two sets screwed on the crossbar move along vertical direction only.

The working principle of this system is sketched in Figure 11. When the magnets are perfectly faced, the repulsive force has a null vertical component, but as soon as the crossbar (and its magnets) moves in the vertical direction, a vertical component of the magnetic force appears. Considering a small relative displacement (Dy), the vertical component of the repulsive force (F_y) is proportional to Dy. We can write

$$Fy \approx F0*(\Delta y/d)$$

where F_0 is the module of the repulsive force and d is the magnet separation. Such a device is equivalent to a vertical spring with a negative elastic constant (anti-spring) whose module is F_0/d. On a seismic filter the magnetic anti-springs act on the crossbar in parallel with the blade mechanical springs, so that the overall elastic constant is reduced and the vertical mode frequencies of the chain are confined below the highest frequency of the horizontal ones.

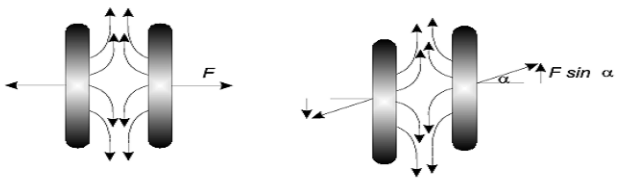

Figure 11. working principle of the magnetic anti-spring system. When the magnets are displaced in the vertical direction (right side) a vertical component of the repulsive force appears.

3.4 Last filter (Filter 7) and Mirror Payload (marionette, mirror and reference mass)

The last mechanical filter of the chain is the so called "Filter 7"[11]. The Mirror Payload, constituted by the *marionette*[12], the *mirror* and its *reference mass*, is suspended from Filter 7 (Figure 12).

The Filter 7 has been designed to steer the payload. It consists of a standard filter to which four aluminum legs (about 900 mm long and 250 mm in diameter) are bolted under the body bottom part. These legs are used as a mechanical support of the coils mounted in front of the permanent magnets screwed on the marionette wings. The coil-magnet pairs are used to apply forces and torques to the marionette, controlling its position in three degrees of freedom: translation along the beam direction (z), rotation around the vertical (θ_y) and transverse (θ_x) axes.

The mirror and its reference mass are independently suspended from the marionette in a cradle formed by a pair of 1.9 m-long thin wires (with an effective pendulum length of 70 cm).

Another set of coil-magnet actuators allow applying forces directly between the reference mass and the mirror, along z, x, θ_x and θ_y for automatic alignment and locking purposes. To this aim, four small magnets are glued to the back face of the mirror and two on the mirror sides. Each magnet is faced by a small coil actuator mounted on the Reference Mass body.

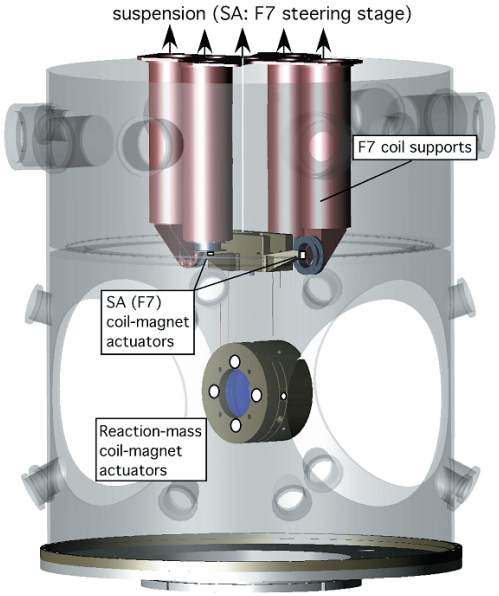

Figure 12. 3D view of the SA lower stage (Marionette and Payload)

4. CONTROL

A hierarchical control strategy is adopted to further reduce the mirror swing, and therefore the control noise[13]. Between 10 mHz and 200 mHz the suspension normal modes relative to the displacement of the top stage in the horizontal plane are damped using a digital active control of the Inverted Pendulum called "Inertial Damping" (ID) [14].

For this reason the top stage is equipped with the following sensors and actuators:

- 3 LVDT (Linear Variable Differential Transformer) displacement sensors[15], set in pin wheel configuration; the secondary windings stay on the inner structure, while the primary ones are rigidly connected to the top stage;
- 3 horizontal Force Balance Accelerometers[16];
- 3 horizontal coil-magnet actuators, set in pin wheel configuration. The coils, arranged as Helmholtz pairs, stay on the inner structure, while the magnets are rigidly connected to the top stage.

Thanks to the inertial damping, the velocity of the low frequency swing of the mirror along the beam is reduced below a few tenths of micrometer per second.

Figure 13 shows a comparison between the open loop and closed loop top stage acceleration. This allows for locking of the interferometer at its operation point and reduces the force to be applied at the mirrors level to maintain the interferometer in the working position[17].

The large (hundreds of microns) ultra-low frequency (below 10 mHz) mirror displacement caused by thermal drifts and Earth tides is compensated using the interferometer as position sensor and the top stage three coil-magnet pairs[13]. The electro-mechanical noise introduced by the required large actuation force is attenuated by the high passive isolation provided by the pendulum chain underneath.

Between 200 mHz and a few Hz, the residual payload displacement along the beam (about one micron after the action of the Inertial Damping and tidal control) is reduced acting on the mirror from the Marionette. Again the induced electro-mechanical noise floor is suppressed down below the sensitivity curve by the mirror pendulum underneath.

Above a few Hz, the few nm residual displacement of the payload is compensated using the Reference Mass actuators that push directly on the mirror.

4.1 Suspension control electronics

Each Virgo Superattenuator has a dedicated suspension control unit constituting by several electronic boards for data conversion, processing and communication, located in a VME crate.

Two Digital Signal Processing (DSP) boards compute the control signals in real-time using digital filters. They are triggered at 10 kHz by the timing distribution system to read error signals from Analog to Digital Converter (ADC) boards and to write back to Digital to Analog Converter (DAC) boards the correction signals. The digital filters used have typically 100 poles and require each a sustained rate of about 10 million floating point operations per second (MFlops). The overall computing power required for all the Superattenuators is in the range of 200 MFlops.

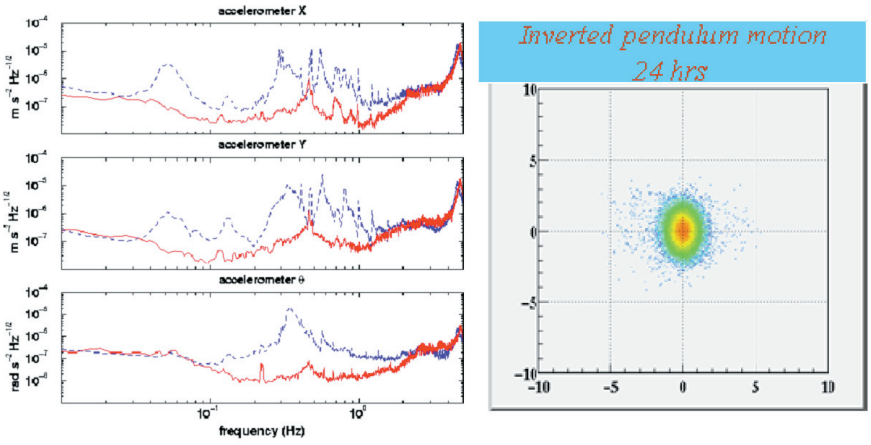

Figure 13. Left: reduction of the Top Stage acceleration consequent to the engagement of the inertial Damping control (blue to red). The plots show the acceleration measured along two horizontal orthogonal directions and the angular acceleration around the vertical axis.
Right: distribution of the Top Stage position in the horizontal plane measured during one day with Inertial Damping engaged. Axes units are micrometers. The red spot contains 90% of the statistics.

The coils used for mirror and marionette actuation are fed with a suitable current generated by coil driver circuits. These convert the voltage control signal in to a current flowing in the coil. The coil drivers have two electronic channels in order to

allow the use of large control signals during lock acquisition and reduced ones with a low noise level when the lock is acquired. These electronic channels are called High Power (HP) and Low Noise (LN) respectively.

5. MEASUREMENT OF THE SEISMIC ATTENUATION PERFORMANCE

The residual displacement at the mirror level is extremely small even if strong excitations are applied to the SA top stage. Consequently, a direct measurement of the total transfer function with commercial instruments is not possible.

5.1 First measurement of Superattenuator performances

We obtained the total transfer function using the transfer function measurements of the single stages[18]. We measured the transfer function matrices using commercial accelerometers, and, connecting the displacements along all the degrees of freedom of each pair of consecutive filters, we estimated the total attenuation. We report in Figure 14 the total transfer function computed with this stage by stage measurement technique. The curve represents an indirect evaluation of the total transfer function, that is the fraction of ground seismic noise (assumed to be isotropic) that is transmitted to the mirror. The measured isolation for vertical and horizontal seismic noise is in excellent agreement with the mechanical simulation and it is large enough to reduce seismic noise below the Virgo sensitivity curve, starting from about 3 Hz.

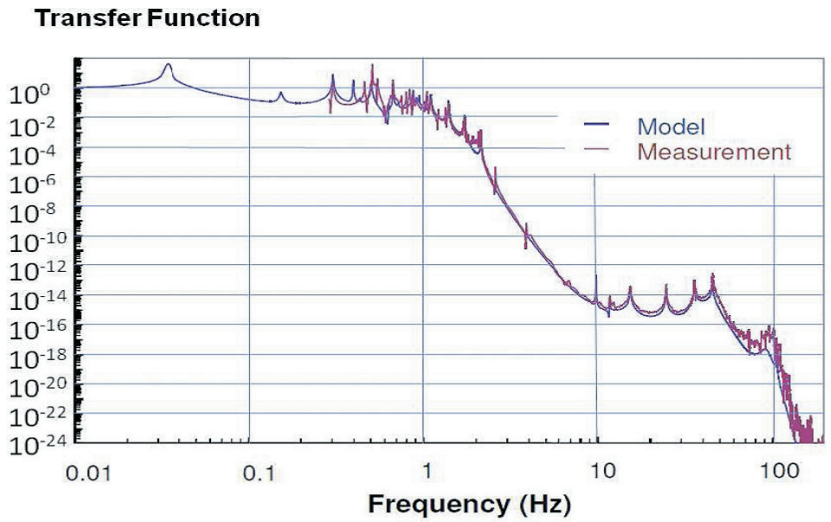

Figure 14. the total Superattenuator transfer function extrapolated by the stage by stage measurements. This quantity has to be multiplied by the input seismic noise detected at the ground level, assumed to be isotropic, to obtain the residual mirror displacement along the beam.

5.2 ATTENUATION MEASUREMENTS IN THE VIRGO INTERFEROMETER

In order to obtain a direct measurement of the filter chain attenuation, we applied several sinusoidal excitations to the SA top stage (both in vertical and horizontal) with frequencies in the Hz and tens of Hz range and we used the interferometer to measure the motion transmitted to the mirror[19]. Once the interferometer is locked, this motion can be measured using the feedback voltage applied to the reference mass coils of the Mirrors to keep the interferometer locked on the dark fringe.

A line in the spectrum of the coil voltage that has the same frequency of the excitation line applied to the top stage can be attributed to the feedback compensation for the residual excitation of the mirror.

The top stage can be excited in the horizontal plane by injecting current into the three coil-magnet actuators used for the Inertial Damping. The sets of three LVDT sensors and of three accelerometers provide two independent measurements of the

displacement of the suspension point in the horizontal plane. The measurements of the amplitude of excitation lines made by different sensors turn out to be equal with an accuracy of a few percent.

The effects of the top stage vertical vibrations on the interferometer can be measured with the same strategy. Two coil-magnet actuators assembled on the Filter Zero are used to excite the suspension point of the filter chain in the vertical direction. Two vertical accelerometers and a LVDT sensor monitor its vertical motion in three independent ways. Once again, the measurements by different sensors at the line frequencies are equal within an accuracy of a few percent, while the noise floor of accelerometers is smaller.

Each measurement required the interferometer locked for several hours, close to its best sensitivity. Moreover, only a single frequency excitation has been applied to the top stage in each experiment, in order to maximize the excitation at the investigated frequency without saturating the coil-magnet actuators and accelerometers. As a consequence the entire set of measurements required a significant amount of interferometer commissioning time.

The result of a typical experiment (with the specific excitation of the top stage at 32.3 Hz along the beam) is reported in Figure 15. The linear spectral density of the top stage displacement measured by accelerometers (gray curve) is here compared with the mirror displacement detected by the interferometer (black curve).

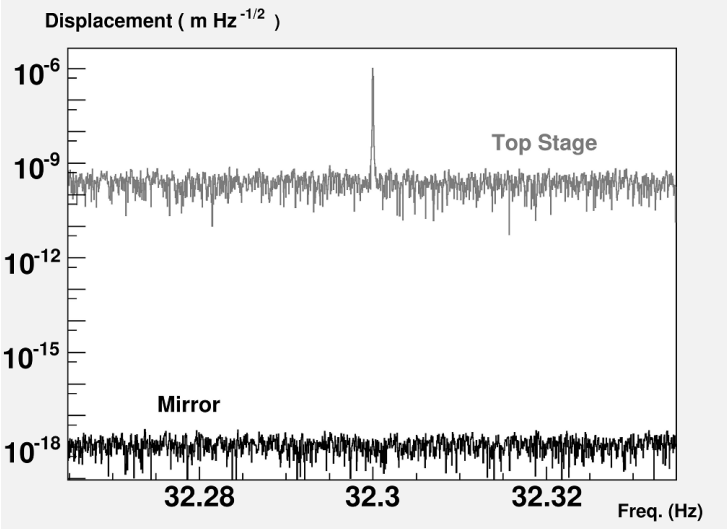

Figure 15. the top stage of the Virgo West cavity terminal Superattenuator is shaken along the beam direction at 32.3 Hz. The linear spectral density of top stage displacement along the beam is compared with the mirror one.

One can see that the latter is dominated by the antenna noise. Since no peak is distinguished from the noise at the mirror level, the ratio between the floor and the top stage peak amplitude gives the upper limit of the transfer function of the filter chain at this frequency.

In almost all the experiments no peak has been detected at the level of the interferometer (Figure 16)

For three cases only, around 30 Hz, a peak at the excitation frequency has been distinguished from the interferometer noise floor. However, also in these experiments, the transfer function has been measured to not exceed a few 10^{-10}, and is thus within the requirements for Virgo and the planned Advanced Virgo (AdV) upgrade.

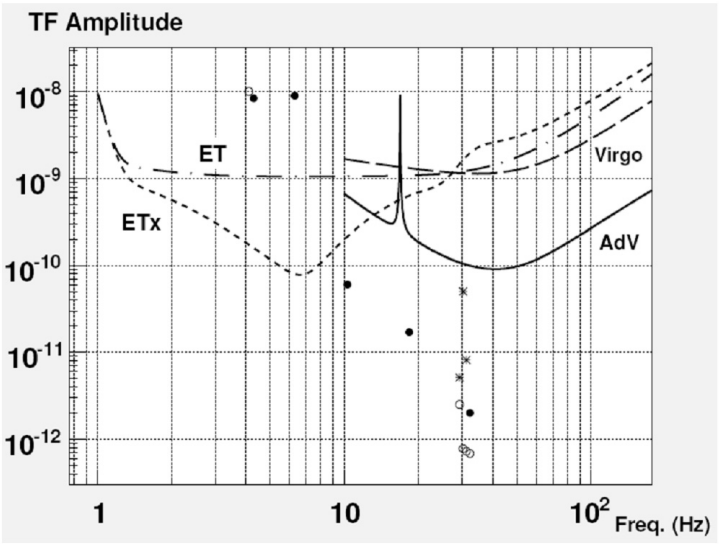

Figure 16. the transfer functions measured in the various experiments compared to the requirements of Virgo and its planned upgrade Advanced Virgo. The circles indicate the upper limits (full circles: excitations along the beam, open circles: vertical excitations).
In three frequencies only (stars point) a peak has been detected at the mirror level (with the excitation of the top stage along the beam direction).

Facing a so accurate measurement (aimed to distinguish a residual excitation on one part on 10^{11} only) the possibility that other mechanisms could cause the detected thin mirror motion, by-passing the extremely high mechanical attenuation, has to be taken into account. The weak transmission between the top stage actuation coils and the mirror could be induced by spurious couplings between cables and/or electronic boards, or by *antenna effects* between the excitation top-stage coils and the coils used for the payload control.

The transfer function of the filter chain for the investigated frequencies above 10 Hz is below the requirement curve also for all the planned European future detectors Einstein Telescope (ET) and its evolution Et-xylophone (Etx), see

http://www.et-gw.eu/presentation.

The measured upper limits below 10 Hz are not sufficient to state that at the investigated frequencies the filter chain alone is not enough to suppress the seismic noise below the Einstein Telescope sensitivity; it is important to stress that in this region only upper limits have been set and that the expected transfer function will be likely much smaller, in agreement with the indirect stage by stage measurement reported in Figure 14.

6. CONCLUSIONS

The suspension system developed to isolate the optical components of Virgo GW interferometer from seismic noise has been deeply tested and characterized, during the commissioning phase and the recent test runs.

An indirect evaluation of the attenuation performance has been obtained with successive measurements on each single SA filter, and it is well in accordance with the mechanical simulations.

Moreover the suspension point of the Virgo Superattenuator filter chain has been excited several times both in horizontal and in vertical directions, injecting sinusoidal signals at different frequencies into the top stage coil-magnet actuators. In almost all the measurements, the mirror residual motion at the excitation frequency is too small to be distinguished from the interferometer noise floor, and only upper limits for the transfer function have been set.

At all investigated frequencies, the transfer function of the filter chain (measured directly or by upper limits) is within the requirements of Advanced Virgo, whose

detection band starts from 10 Hz. Above this frequency the measured attenuation is compliant with the requirements of the third-generation detector Einstein Telescope. This future interferometer is actually less demanding in terms of attenuation, at frequency above 10 Hz, because the seismic noise is much lower underground.

Minor changes to the Superattenuator design (such as an increase of the chain length) will be necessary for Einstein Telescope only if the detection threshold frequency is moved below 3 Hz.

REFERENCES

[1] P.R.Saulson - *Fundamentals of Interferometric Gravitational Wave Detectors* World Scientific, ISBN 9810218206 (1994)

[2] LIGO, http://www.ligo.caltech.edu

[3] GEO, http://www.geo600.org

[4] TAMA, http://tamago.mtk.nao.ac.jp/tama.html

[5] Virgo, http://www.virgo.infn.it

[6] P.R.Saulson, Phys. rev. D 42 (8), 2437-2445 (1990)

[7] The Virgo Collaboration, Virgo Final Design, E.T.S., Pisa, Italy (1995)

[8] S. Braccini et al., Meas. Sci. Technol. 11, 467-476 (2000)

[9] M. Beccaria et al., Nucl. Instrum. Methods Phys. Res. A 394, 397 (1997)

[10] S. Braccini et al., Rev. Sci. Instrum. 64, 310 (1993)

[11] G. Ballardin et al., Rev. Sci. Instrum. 72, 3635-3642 (2001)

[12] A. Bernardini et al., Rev. Sci. Instrum. 70, 3463 (1999)

[13] F. Acernese et al., Astrop. Phys. 20 (6), 629-640 (2004)

[14] G. Losurdo et al., Rev. Sci. Instrum. 72, 3653 (2001)

[15] H. Tariq et al., Nucl. Instrum. Methods A 489, 570 (2002)

[16] S. Braccini et al., Rev. Sci. Instrum. 66 (3), 2672 (1995)

[17] F. Acernese et al., Class. Quantum Grav. 19, 1631 (2002)

[18] G. Ballardin et al., Rev. Sci. Instrum. 72 (9), 3643-3652 (2001)

[19] F.Acernese et al., Astrop. Phys. 33 (3), 182-189 (2010)